

Estimation of Aerodynamic Stability Derivatives for Space Launch System and Impact on Stability Margins

Jing Pei^{*}

NASA Langley Research Center, Hampton VA 23681

John Wall[†]

Dynamic Concepts, Inc., Huntsville, AL, 35806

This paper describes the techniques involved in determining the aerodynamic stability derivatives for the frequency domain analysis of the Space Launch System (SLS) vehicle. Generally for launch vehicles, determination of the derivatives is fairly straightforward since the aerodynamic data is usually linear through a moderate range of angle of attack. However, if the wind tunnel data lacks proper corrections then nonlinearities and asymmetric behavior may appear in the aerodynamic database coefficients. In this case, computing the derivatives becomes a non-trivial task. Errors in computing the nominal derivatives could lead to improper interpretation regarding the natural stability of the system and tuning of the controller parameters, which would impact both stability and performance. The aerodynamic derivatives are also provided at off nominal operating conditions used for dispersed frequency domain Monte Carlo analysis. Finally, results are shown to illustrate that the effects of aerodynamic cross axis coupling can be neglected for the SLS configuration studied.

I. Introduction

Space launch vehicles with cylindrical shapes similar to NASA's Space Launch System (SLS) are typically aerodynamically unstable because the center of pressure (CP) is forward of the center of gravity (CG). Therefore, a closed loop control system is required to provide active stabilization. Proper estimation of aerodynamic stability derivatives is essential to accurately assess the natural stability of the system so that control system parameters can be selected to maintain acceptable control margins¹. Traditionally, stability derivatives are computed about the nominal operating conditions using finite differencing methods (forward, backward, or central differencing). Recent ascent aerodynamic databases from Ares I-X and I suggest that all the aforementioned methods should yield similar results given the linear behavior of the aerodynamic coefficients for relatively small angles of attack (α) and sideslip (β). However if proper adjustments are not applied to the uncorrected wind tunnel data during the generation of the database, artificial behaviors such as nonlinearities and asymmetry could appear in the final coefficients. As a result, appropriate judgment is required to properly estimate the derivatives.

^{*}Aerospace Engineer, Vehicle Analysis Branch, NASA Langley Research Center, Hampton VA

[†]Aerospace Engineer, Dynamic Concept Inc., Huntsville AL

In the case of coefficients exhibiting nonlinear behavior over the range in which the control system operates, choosing the coefficients at the higher angles while determining the derivatives may result in over or under estimation of the true gradient around the control trim α and β . If asymmetry exists in the data, the three finite differencing techniques produce significantly different results. Finally, it is important to correctly capture the normal force coefficient slope (CN_α) at $\alpha = 0$ in the pitch plane and side force coefficient (CY_β) at $\beta = 0$ in the yaw plane. When using forward or backward differencing techniques, a small deviation in CN_α and CY_β leads to significant variations in pitching moment slope CM_α ($\delta M/\delta \alpha$) and yawing moment slope Cn_β ($\delta Cn/\delta \beta$) about the center of gravity. These points will be illustrated in the paper.

Stability derivatives for the SLS crew vehicle discussed in this paper were estimated using the Design Analysis Cycle 2 (DAC-2) static ascent force and moment aerodynamic database which was based on the 0.5% scale wind tunnel test² conducted at NASA Marshall Space Flight Center. These derivatives are tabulated as a function of Mach number, angle of attack, and angle of sideslip. The derivatives were computed about $\alpha/\beta = 0$ at nominal operating condition through the boost phase of flight where aerodynamic stability considerations are significant.

In the sections that follow, the implications and methods associated with computing the aerodynamic stability partial derivatives are discussed. Section II uses a simple planar model to demonstrate the aerodynamic instability associated with a typical launch vehicle. It is intended to illustrate the impact of the stability derivatives on the choice of controller gains and the resultant stability margins. Section III describes the methodology involved in the computation of the stability derivatives for the boost phase of the SLS crew vehicle accounting for the lack of smoothness and nonlinearities present in the database. Frequency domain and stability margin results are presented in Section IV, and Section V illustrates the lack of aerodynamic coupling amongst the three axes for this configuration. Note only pitch plane results are shown in this paper; similar analyses were applied to the yaw axis.

II. Background and Motivation

The SLS flight control system is commanded to follow a prescribed zero angle of attack (zero lift) gravity turn ascent trajectory prior to booster separation in order to minimize aerodynamic loads as it passes through the region of high dynamic pressure. The nominal stability derivatives are therefore computed about zero α/β , the point about which the controller operates. Gains for the linear proportional-integral-derivative (PID) control system are designed to provide good rigid body stability and command tracking properties with the aid of discrete input filtering, and avoiding adverse interaction with the propellant slosh and structural dynamics. A desired closed loop frequency (bandwidth) is specified by the control designer often as a compromise to meet the conflicting stability and performance metrics. Equation 1 shows a simplified version of the closed loop system where PD (proportional-derivative) feedback is applied to an aerodynamically unstable rigid body in the pitch plane.

$$\frac{\theta}{\theta_c} = \frac{C_2(K_D S + K_P)}{S^2 + K_D C_2 S + (K_P C_2 - C_1)} = \frac{C_2(K_D S + K_P)}{S^2 + 2\xi_c \omega_c S + \omega_c^2} \quad (\text{Eq. 1})$$

$$C_1 = \frac{Cm_{\alpha, cg}}{I_{yy}} \text{ and } C_2 = \frac{Cm_{\delta, cg}}{I_{yy}}$$

C_1 is the normalized pitching moment coefficient gradient. C_2 represents the normalized control moment coefficient gradient. The proportional gain K_p and derivative gain K_D are chosen to provide a desired control frequency ω_c and damping ratio ξ_c . Typically, ω_c is on the order of 0.8 rad/s and ξ_c ranges from 0.4 to 0.8 for good closed loop performance³. As modifications to PD gains are made and parasitic effects such as actuator, slosh, and flexible dynamic models are incorporated, basic aerodynamic stability and desired bandwidth provide a rough guideline for total system gain, K_T . Pitch plane low frequency stability is dominated by the aerodynamic derivatives associated with the rotational dynamics of the launch vehicle about the CG, $Cm_{\alpha, cg}$. A positive $Cm_{\alpha, cg}$ indicates negative pitch stiffness and an aerodynamically unstable vehicle which is illustrated as a pair of real poles (one stable and one unstable) on the root locus. Stabilization through artificial control is required to bring the unstable pole to the left hand plane. As can be seen by the sign of the lowest order term in the denominator of Equation 1, for a given positive magnitude of C_1 , K_p must be sufficiently large to ensure stability of the closed loop system ($K_p C_2 > C_1$). Errors in modeling $Cm_{\alpha, cg}$ could lead to the improper interpretation regarding the natural stability characteristics of the system.

Figure 1 is a typical Nichols chart used to evaluate the frequency domain stability margins of the conditionally stable launch vehicle. The low frequency or aerodynamic gain margin is measured at the frequency where the open loop phase initially crosses -180 degrees. This indicates that the system is naturally unstable and it is conditionally stable as long as the loop gain stays above a certain threshold, hence a finite value of gain margin. The rigid body gain margin, driven primarily by required bending filter attenuation/lag, slosh modes, and servo-actuator lag, is measured at the second -180 degree crossing. The value of the gain at the second phase crossover marks the upper bound for the total loop gain. The phase margin is the difference between the value of phase and -180 at the gain crossover frequency. The disc⁴ which encompasses the (0dB, 180deg) critical point is defined by the 6 dB of gain and a 30 degree phase margin design criteria, as used for Space Shuttle and Ares programs. Due to significantly high structural modal gains, the total system gain must be kept relatively low. This decreases the available aerodynamic stability margin, leaving little room for excess conservatism in the aerodynamic partial derivative estimates.

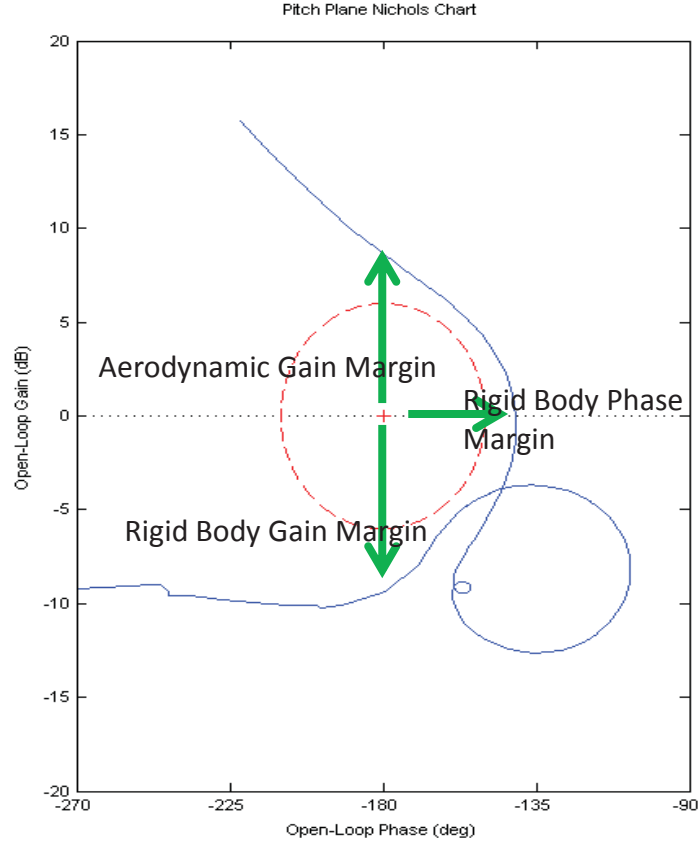


Figure 1. Sample Nichols Chart and Definitions

It can be clearly seen from Equation 1, an over estimation in the value of $CM\alpha_{cg}$, represents a more aerodynamically unstable vehicle which would require a higher minimum K_p gain to achieve the desired ω_c . This scenario indicates a reduced nominal aerodynamic gain margin but improved performance (command following and disturbance rejection) due to a large value of K_p . On the contrary, under estimating the nominal $CM\alpha_{cg}$ (less aerodynamically unstable vehicle) requires a smaller minimum K_p which indicates an increase in the nominal gain margin but negative impact on the performance. These results are most significant in the transonic flight regime and other regions of high dynamic pressure (Q_{bar}) when aerodynamic forces and moments are greatest. Figure 2 shows the nominal Mach vs. Q_{bar} profile for the TR2A⁴ trajectory during the atmospheric boost phase.

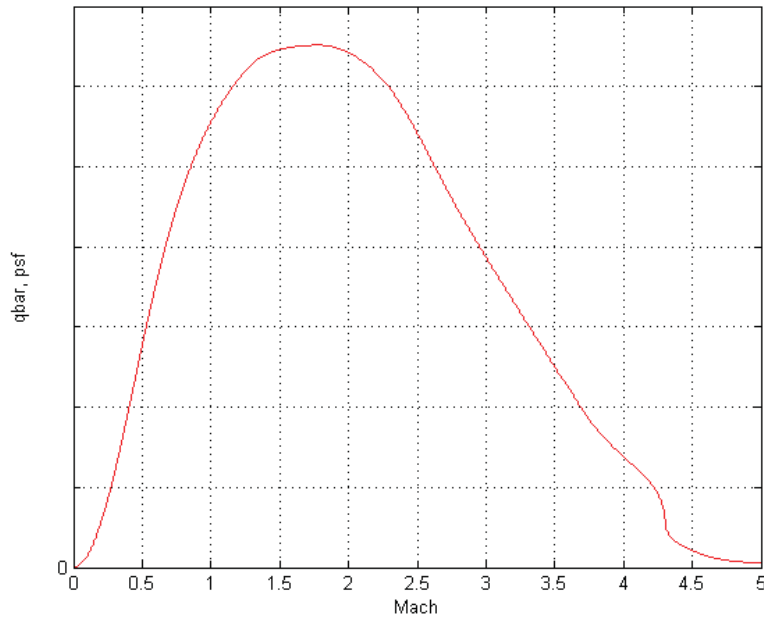


Figure 2. Nominal Mach vs. Qbar profile

III. Aerodynamic Database Results

The boost portion of the aerodynamic force and moment database was generated using wind tunnel test data from the NASA Marshall Space Flight Center 14 inch Tri-sonic wind tunnel facility. Most of the vehicle major protuberances were modeled. In the early stage in the SLS design cycle, a relatively small model was tested which diminished the fidelity of the database. The data was collected at total angle of attack (α_T) sweeps for a constant roll angle (ϕ) and Mach number. For the construction of the final database, the processed data was mapped onto a uniform α/β grid ranging from -8 to +8 degrees with a 2 degree increment. The Mach number breakpoints range from 0.3 to 4.96 with fine increments in the transonic regime and maximum Qbar regions and with sparse increments past Mach 2.5. Figure 3 shows the SLS 10003 configuration full stack wind tunnel model.



Figure 3. SLS 10003 Crew Configuration

Figure 4 is a plot of C_N versus α at Mach 1.05. While curve fitting and smoothing was not applied to the wind tunnel data during the generation of the database, it is apparent that the final coefficient is slightly nonlinear across the range of angle of attack. A noticeable difference in the absolute value of C_N between positive and negative α is observed. In addition, there appears to be an offset at $\alpha = 0$. For a symmetric configuration, aerodynamic loading should be nearly zero at $\alpha = 0$. However, the offset at $\alpha = 0$ may be attributed to protuberances such as LH_2 and LO_2 fuel feedlines. Since the vehicle operates about a zero α condition for the portion of the ascent trajectory and for which aerodynamic influences are important, the gradient of the pitch plane coefficients about $\alpha = 0$ is used in the design of the pitch axis stability margins. Lack of smoothness in the database presents a challenge in determining the aero coefficient slope which is very sensitive to the range of α selected for finite differencing. Visual inspection of the C_N versus α curve indicates that the slope at $\alpha = 0$ varies depending on the range of α used. For instance, 0 to 2 degrees data yields a smaller slope as compared to 0 to 4 degrees, etc.

During DAC-1 analysis, the approach taken in the control stability analysis is illustrated in Figure 4. In this approach, denoted hereafter as the “DAC-1 approach”, C_N is assumed be zero at $\alpha = 0$ and uses the average slope between $\alpha = (0,7), (0,5), (0,3), (0,1)$ to determine $C_N\alpha$ at $\alpha = 0$. The assumption that $C_N = 0$ for $\alpha = 0$ was valid with the first release of the database, but was not true in the higher fidelity second release with its y-offsets. When applying this assumption to the DAC-2 database along with the lack of smoothness in the coefficients, resulted in incorrectly estimated stability derivatives.

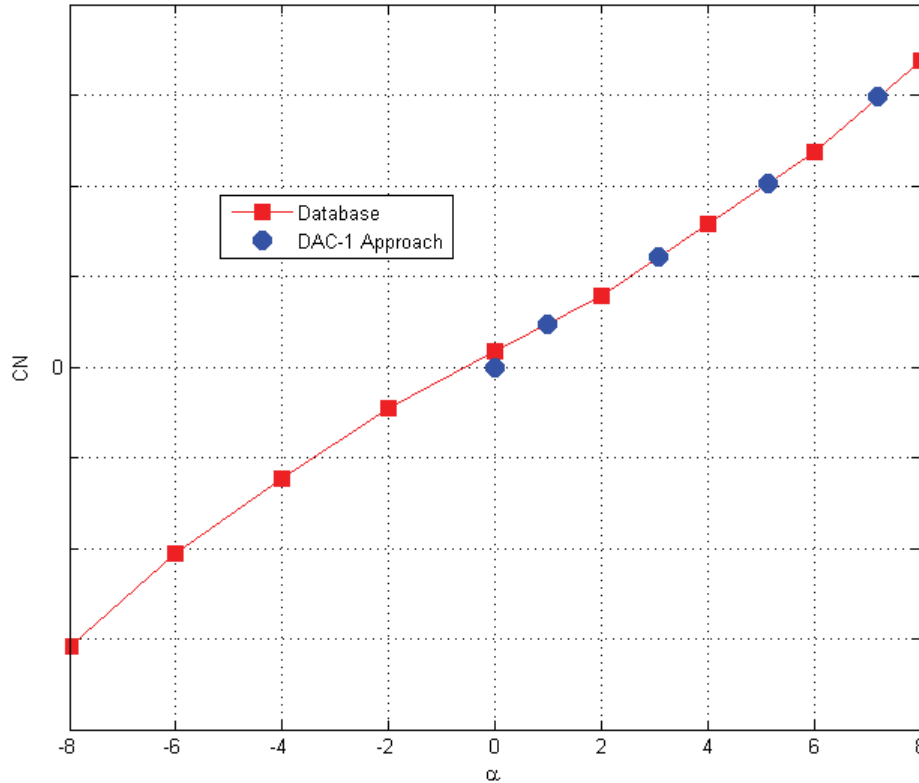


Figure 4. C_N vs. α at Mach = 1.05, $\beta = 0$

The aerodynamic force and moment coefficients in the database are provided about the moment reference point (MRP) which is located near the base of the core stage. Pitching moment gradient about the vehicle instantaneous center of gravity, $CM_{\alpha, cg}$, is computed across the Mach number breakpoints in the database by transferring the pitching moment about the MRP to the CG (the transfer distance is denoted by X_{mrp2cg}) using Equation 2. $CM_{\alpha, cg}$ provides an indicator regarding the natural stability of the vehicle. This is equivalent to providing normal force coefficient gradient with an associated center of pressure location, the format adopted during Saturn V⁵. It is apparent from Equation 2 that an increase in CN_{α} leads to a smaller value of $CM_{\alpha, cg}$, representing a reduction in pitch plane instability.

$$CM_{\alpha, cg} = CM_{\alpha, mrp} - X_{mrp2cg} \cdot CN_{\alpha} \quad (\text{Eq. 2})$$

Figures 5 and 6 illustrate the stability partial derivatives resulting from finite differencing for several different ranges of α . Large differences amongst the methods can be observed. Using the ± 2 deg data yields the largest value for $CM_{\alpha, cg}$. As the range of α increases, $CM_{\alpha, cg}$ decreases. The “mean” approach is the average of the first six methods. The DAC-1 method over estimates CN_{α} which translates to a reduced values of $CM_{\alpha, cg}$; it predicts that the vehicle is aerodynamically stable in the pitch plane up to Mach 1.1, neutrally stable at Mach 1.1, unstable from Mach 1.2 to 2, and stable beyond Mach 2. This is in conflict with the other methods which indicate that the vehicle is aerodynamically unstable up to Mach 2.5 resulting from its incorrect assumption that $CN = 0$ at $\alpha = 0$. The large variations in the values of $CM_{\alpha, cg}$, especially from Mach 0.8 to 1.6 amongst all the methods, were deemed to be physically unrealistic. The SLS aerodynamics team collectively agreed that these observations were artificial and attributed to the lack of corrections applied to the wind tunnel data during the generation of the database. Aerodynamic slender body theory suggests that for wings of low aspect ratio or slender fuselages (length \gg diameter), the pitch axis coefficients should be linear for small angles of attack. In addition, previous flight qualified launch vehicles databases such as Saturn V, Ares I-X and I⁶, all suggest that CN and CM are linear over an α range of ± 6 degrees. Therefore, the various methods shown in Figure 6 should all predict similar $CM_{\alpha, cg}$ values.

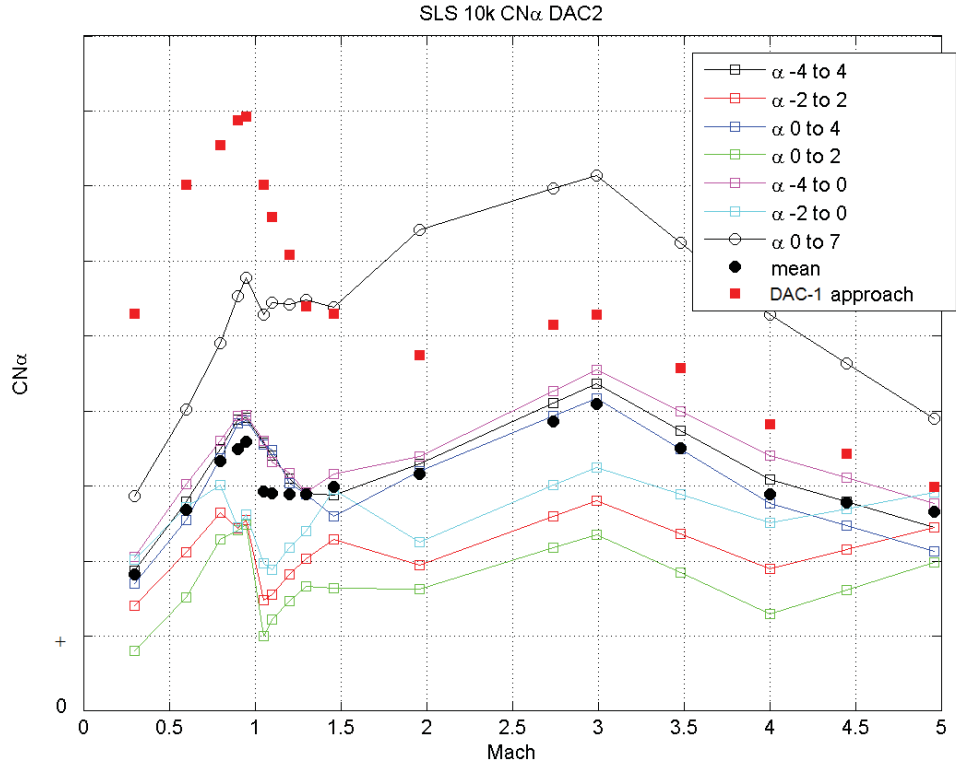


Figure 5. CN_{α} vs. Mach

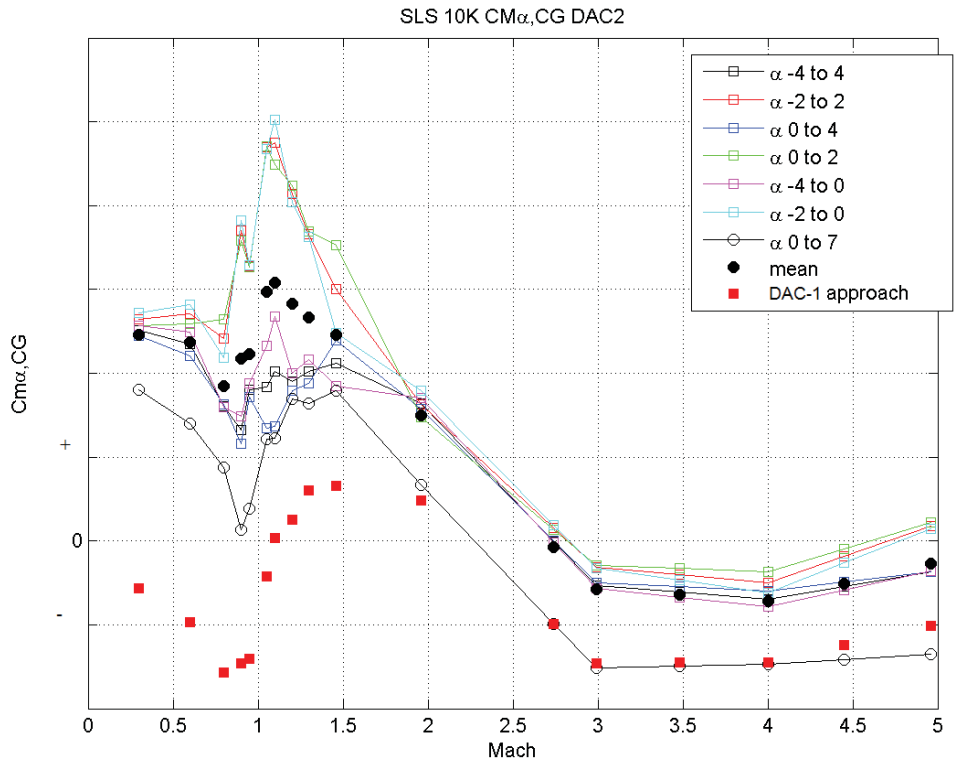


Figure 6. $CM_{\alpha,CG}$ vs. Mach

The “mean” $CM_{\alpha, cg}$ values shown in Figure 7 at $\alpha/\beta = 0$ were used to derive the corresponding center of pressure locations and provided, along with the nominal center of gravity time history in Figure 4, an alternative way of representing the vehicle aerodynamic stability. It is apparent that during the boost phase (0 to 120 seconds) the CP is forward of the CG until approximately 90 seconds indicating negative static margin and an aerodynamically unstable vehicle. The greatest amount of static instability occurs slightly before 60 seconds, when the CP is at its most forward location relative to the CG. Thereafter, the CP gradually shifts aft and closer to the CG. This observation is consistent with compressible aerodynamic theory⁶ which suggests that the oblique shock off the vehicle nose lies closer to the body with increasing Mach number which shifts the aerodynamic loading aft.

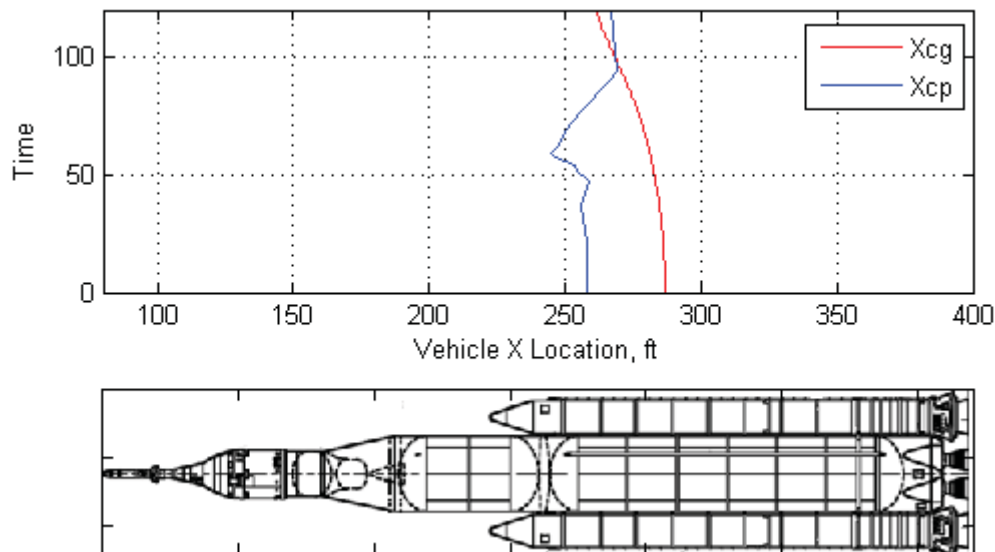


Figure 7. Center of Gravity and Center of Pressure Time History

Figure 8 shows the total normal force coefficient gradient distribution along the x-axis of the vehicle at Mach 1.1 and 3.0. The distributions were derived by taking the high resolution line loads (dC_N/dx) generated by Computational Fluid Dynamics (CFD) and integrating them at discrete x locations along the core stage and the two Solid Rocket Boosters (SRBs). By repeating this process for several angles of attack, the gradients were obtained. It is apparent that the overall aerodynamic loading distribution shifts aft as Mach number increases which is consistent with the CP trend shown in Figure 7.

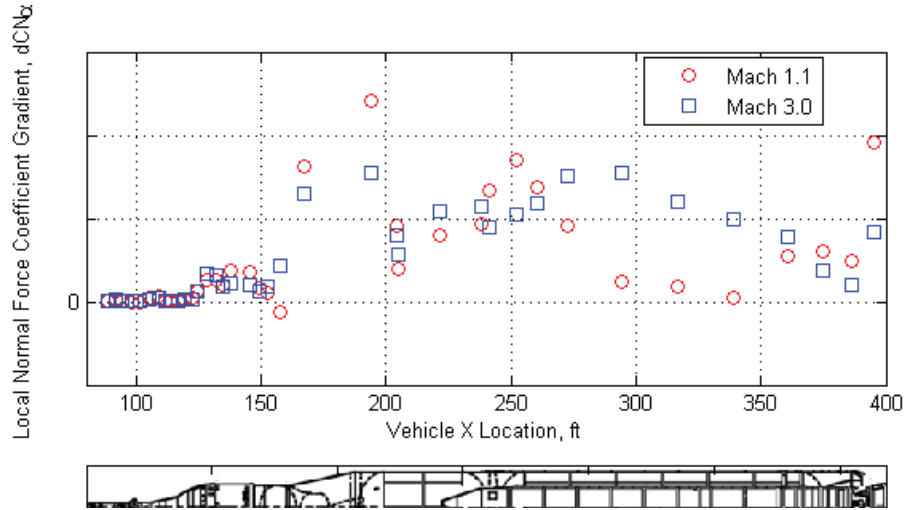


Figure 8. Variation of Local $C_{N\alpha}$ with Longitudinal Position, Mach 1.1 and 3.0

In order to provide an assessment of uncertainty on the aerodynamic stability partials due to operating condition, C_N and C_M slopes were computed at off nominal conditions (non-zero α/β) using a central differencing scheme based on the two nearest data points in the database (2 deg increments). For example, $C_{N\alpha}$ at $\beta = 2$, $\alpha = 2$ was computed using the data at $\alpha = 0$ and 4, $\beta = 2$. Figure 9 shows $C_{M\alpha, cg}$ contour as a function of α and β resulting from this computation. The $C_{M\alpha, cg}$ contour indicates that the vehicle is the most unstable in pitch at $\alpha = 0$ and becomes increasingly stable as α increases indicating that the nominal operating condition produces a conservative upper bound on the partials. Furthermore, the gradient contour indicates that β does not appear to have an appreciable effect on the pitch plane derivatives as there exists no physical mechanism (other than small protuberances) with the configuration at which a pure sideslip could produce normal force.

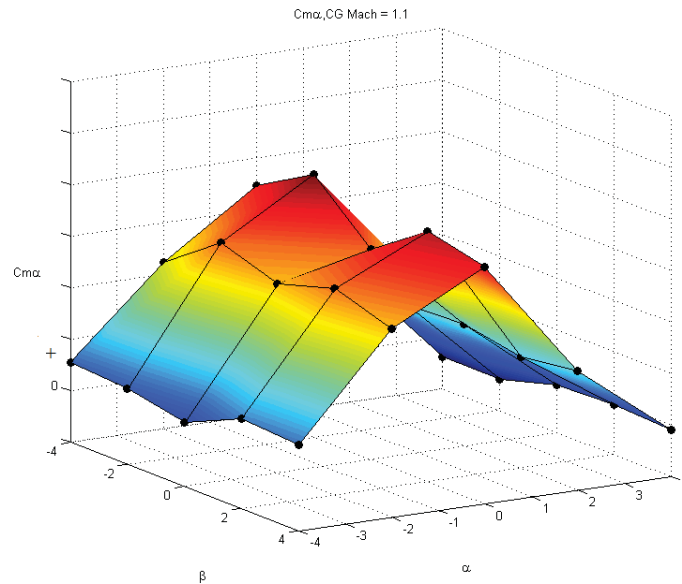


Figure 9. $C_{M\alpha, cg}$ vs. α and β , Mach = 1.1

IV. Frequency Domain Results

The “mean” $CM_{\alpha, cg}$ values shown in Figure 6 were used as the official aero stability partials for the DAC-2 flight control design. Due to the preliminary nature of the database, this decision was made based on the aerodynamic team assessment and conclusion that the spread was too large around the transonic region as discussed in Section III. To be conservative, using the ± 2 deg data would be the obvious choice. However, this translates to a further reduction in aerodynamic (low frequency) gain margin, particularly during the region between transonic and maximum dynamic pressure. Figure 10 is a plot of the pitch stiffness, described by Equation 3, at $\beta = 0$ versus Mach with the Q_{bar} profile superimposed.

$$\text{pitch stiffness} = \frac{CM_{\alpha, cg} \cdot Q_{bar} \cdot S_{ref} \cdot L_{ref}}{I_{yy}} \quad (\text{Eq. 3})$$

Pitch stiffness is a dimensional value that quantifies the degree of instability or stability attributed to aerodynamics. The plot suggests that the vehicle experiences the greatest amount of instability between Mach 1.05 and 1.3, falling outside the maximum dynamic pressure region (Mach 1.5 to 2).

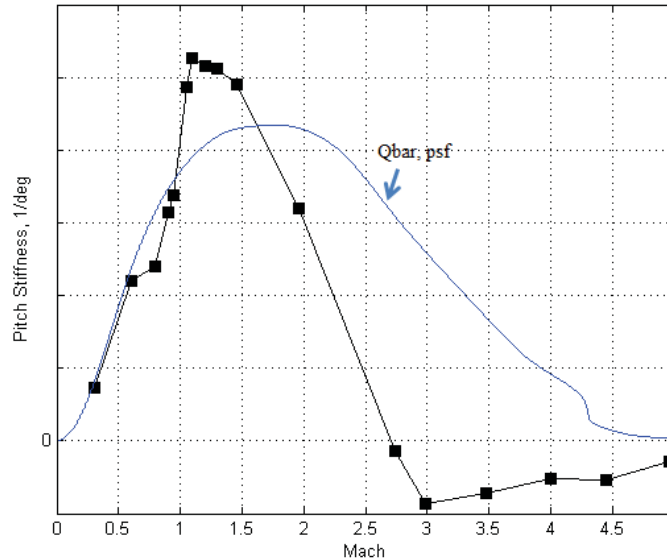


Figure 10. Nominal Pitch Stiffness, $M_{\alpha, cg}/I_{yy}$ vs. Mach

Nichols charts were generated in STARS⁷ (Space Transportation Aeronautics Research Simulation) to examine the frequency domain stability margins. STARS is an MATLAB/Simulink-based simulation developed at NASA Langley Research Center that is being used to provide Verification and Validation of SLS time and frequency domain results. Figure 11 shows a pitch plane Nichols chart generated at $T = 56$ seconds, corresponding to approximately Mach = 1.05. The blue curve is created based on the “mean” stability derivatives shown in Figure 6.

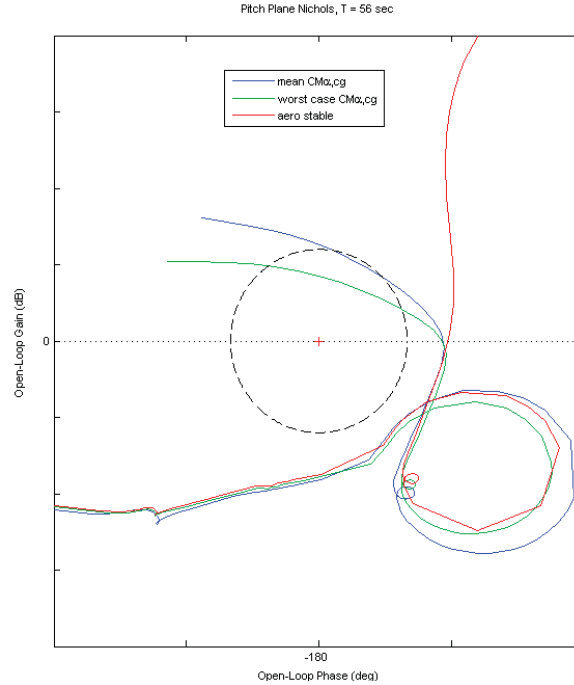


Figure 11. Nichols Chart for Pitch Channel, T = 56 sec

The nominal DAC2 controller design is tightly constrained at Mach 1.05 as seen from the Nichols space. The large value of $M\alpha_{cg}$ leads to a reduction in the low frequency gain margin causing the gain/phase curve to impinge the top of the disc. To maximize time domain performance and recover the low gain frequency margin lost due to increase aerodynamic instability, the control designer seeks to raise the total system gain. However, large system gain causes the curve to impinge the bottom of the disc violating the rigid body and flex attenuation requirements. Using the most conservative value of $CM\alpha_{cg}$ shown in Figure 6 yield in a nominal design that fails to meet the 6 dB low frequency design criteria⁴ and unnecessarily constrain the design already stressed by structural and slosh modes. This case is represented by the green line.

The red curve on Figure 11 is the same pitch plane open loop frequency response at 56 seconds but generated using the stability derivatives derived using the DAC-1 method. The only significant difference between the other two curves is at the low frequency below the gain crossover indicating the range over which the aero data affects the frequency response. The red curve indicates that the vehicle has infinite aerodynamic gain margin since the phase never crosses -180 deg for positive dB gain. One could theoretically de-activate the control system and the vehicle would drift into in a wind disturbance. The observation in the Nichols chart is consistent with the DAC-1 method derived $CM\alpha_{cg}$ value at Mach 1.05 shown in Figure 6, suggesting that the vehicle is aerodynamically stable. This example illustrates that misleading conclusions can be drawn regarding the stability of the vehicle if proper corrections were not applied to the wind tunnel data during the generation of the database. In addition, a small assumption such as $CN = 0$ at $\alpha = 0$ made in the DAC-1 approach could potentially have a significant impact on the assessment of the control margins.

Figure 12 is a co-plot of open loop frequency responses generated at selected time points throughout the atmospheric boost phase. The aero gain margin steadily decreases from 10 to 40 seconds with increasing static aero instability. The yellow line represents $T = 56$ seconds when aerodynamic instability is the greatest and the nominal system barely meets the 6 dB aero gain margin design criteria. In addition, the yellow line encroaches the disc indicating that the design space is severely challenged due to vehicle dynamics⁴. The aero gain margin increases after 56 seconds as aerodynamic instability diminishes. At 92 seconds and beyond, the effect of aerodynamics on vehicle stability can be effectively ignored.

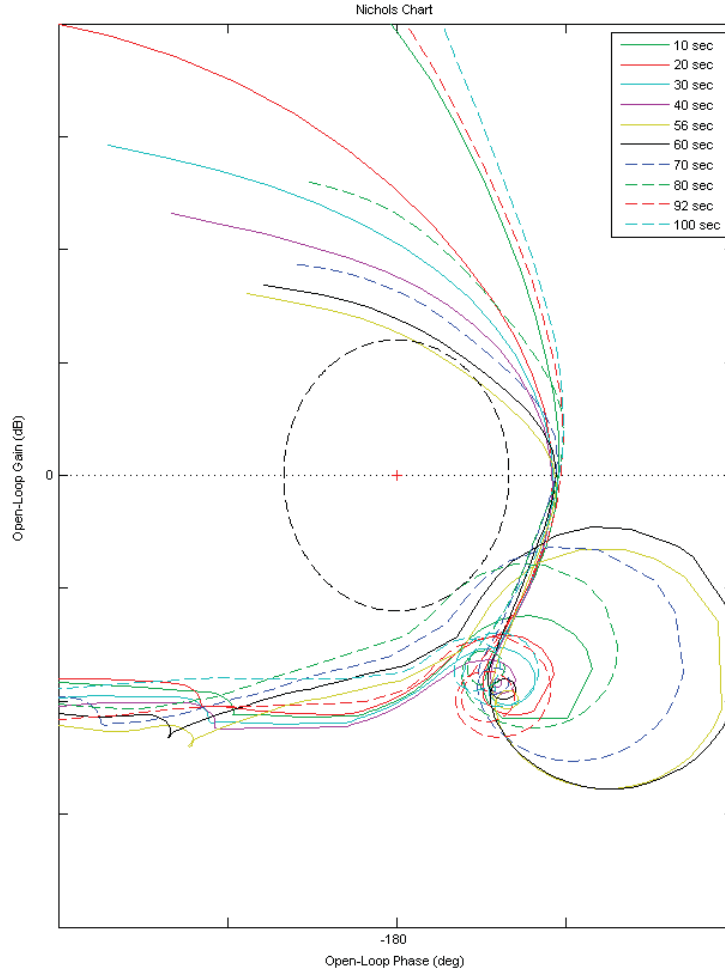


Figure 12. Nichols Chart at Various Time Points

V. Discussion

Cross-axis derivatives terms such as $CM_{\beta, cg}$ and Cn_{α} were computed to assess the degree of aerodynamic coupling amongst the roll, pitch, yaw axes. Figure 13 is a plot of $CM_{\beta, cg}$ at Mach 1.1 illustrating no significant coupling between the pitch and yaw axes. Plots were generated for the other coefficients at other Mach numbers, and the magnitudes of these terms were found to be sufficiently small. Figure 14 is the open loop Bode plot of the pitch channel.

The 2-2 term presents pitch input to pitch output, where as the 1-2 and 3-2 terms indicates roll/yaw input to pitch output. The cross axis magnitude Bode shows minimal gain in the low frequency range for the 1-2 and 3-2 terms (system never crosses the 0 dB line) indicating the insignificance of aerodynamic cross axis coupling. As aerodynamic coupling was found to be negligible, the flight control analysis used only the planar components of the partials.

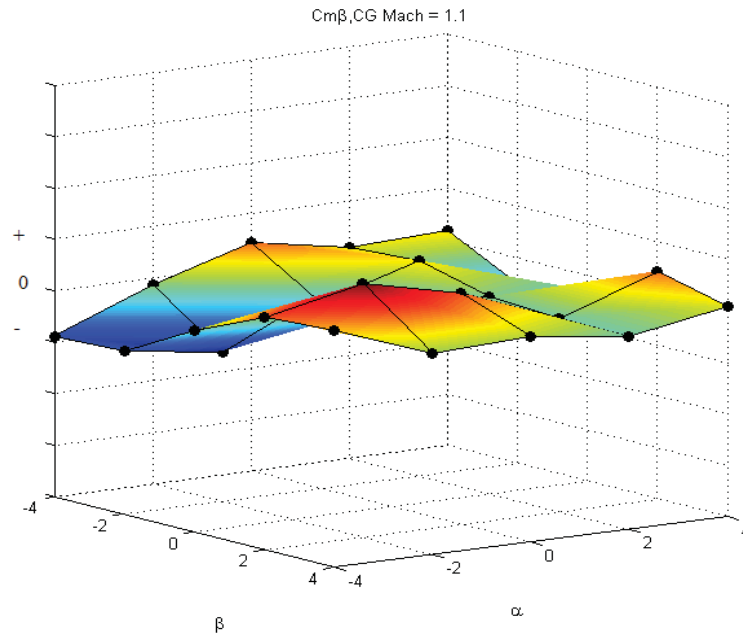


Figure 13. $CM_{\beta,CG}$ vs. α and β , Mach = 1.1

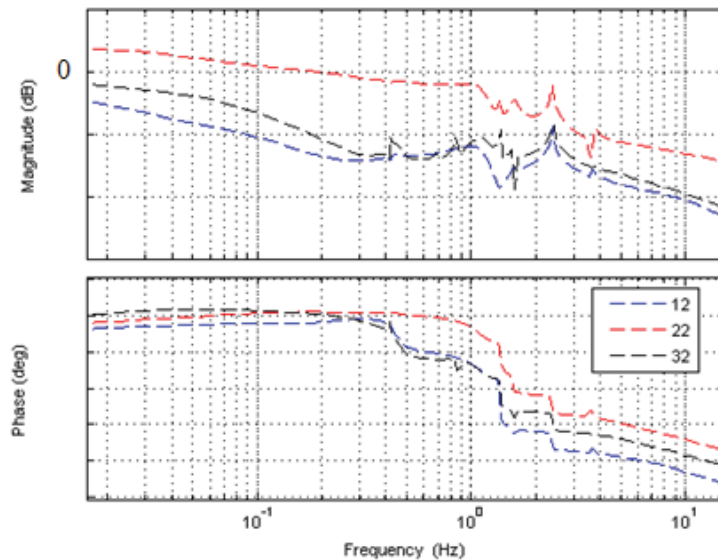


Figure 14. Pitch axis Bode, $T = 56$ sec

VI. Conclusions

Computing stability derivatives from static force and moment aerodynamic database is not trivial when there are nonlinearities and asymmetry present. Careful attention is required to determine whether the observations are artificial or a presentation of the vehicle aerodynamic characteristics. This is especially true in early phases of a flight program during which there is a lack of maturity in the aerodynamic model and insufficient corrections made to the wind tunnel data during the generation of the database. Generally for launch vehicle, the aerodynamics coefficients are linear up to several degrees of α and β . Careful attention should be paid to determine the range of α and β used to compute the derivatives as well as the finite differencing technique. Over or under predicting the derivatives would mislead the control engineer regarding the natural stability of the system. This would lead to improper tuning of the controller gains which would ultimately impact vehicle stability and performance. To truly capture the gradient of the aerodynamic coefficients at about the nominal operating condition, the database should be well defined about $\alpha = 0$. Aerodynamic cross coupling effects are found to be negligible for the SLS configuration. All the issues discussed in this paper are being addressed in the DAC-3 release of the SLS aerodynamic database.

References

- ¹Stevens, B., Lewis, F., "Aircraft Control and Simulation," 2nd edition, 2003.
- ²Purinton, D., "Aerodynamic database SLS-10-D-AFA-002," NASA MSFC/EV33 memo, June 22, 2012
- ³Greensite, A., "Analysis and Design of Space Vehicle Flight Control Systems, Volume VII – Attitude Control during Launch," NASA CR-820, 1967.
- ⁴"Integrated_GNC_Performance_Assessment_PDR_Version_1_May_3.docx". SLS PDR GN&C Databook. May 3, 2013
- ⁵McQuade, P., Schutzenhofer, L., Woods, B. "Principles and Practices of Launch Vehicle Aerodynamics".
- ⁶Pamadi, B., Pei, J. "Aerodynamic Database Development for Liftoff/Transition and Ascent of the Ares I Vehicle". Journal of Spacecraft and Rockets. Vol. 49, No. 4, July-August 2012.
- ⁷"Space Transportation Aeronautics and Research Simulation". Dynamics & Control Branch. NASA Langley Research Center. 2013